

Characterization of Cellulose Nanocrystals Grafted with Organic Acid Chloride of Different Sizes

Aparecido Junior de Menezes^{*1,3}, Elson Longo², Fábio Lima Leite¹ and Alain Dufresne³

¹Department of Physics, Chemistry and Mathematics (DFQM), Federal University of São Carlos, 13052-780, Sorocaba, Brazil

²Institute of Chemistry (IQ), São Paulo State University, Araraquara, Brazil

³Laboratory of Pulp and Paper Engineering, (LGP2) Grenoble-INP PAGORA, 461 rue de la Papeterie CS10065 - 38402 Saint Martin d'Hères Cedex, France

Received August 26, 2014; Accepted November 2, 2014

ABSTRACT: In the work presented in this article surface chemical modification was applied to ramie cellulose nanocrystals by grafting organic acid chlorides presenting different lengths of the aliphatic chain. The objective of this surface chemical treatment was to enhance the nonpolar nature of the grafted nanocrystals and improve their dispersibility in a nonpolar polymeric matrix. The occurrence of the chemical modification was evaluated by Fourier transform infrared (FTIR) spectroscopy, the degree of crystallinity by X-ray diffraction, and the morphology by scanning electron microscopy with field emission gun (FEG-SEM) and atomic force microscopy (AFM). The morphology and crystallinity provided by different experimental methods were carefully compared.

KEYWORDS: Cellulose nanocrystals, surface chemical modification, AFM

1 INTRODUCTION

The use of polysaccharide nanocrystals has gained considerable attention as reinforcement in nanocomposites. This interest is growing because of several advantages such as low density, low cost, renewable character, biodegradability and good specific mechanical properties compared to the traditional reinforcement materials, e.g., glass fiber [1–3]. Cellulose nanocrystals can be obtained by hydrolysis with sulfuric acid of the biomass, resulting in stable aqueous suspensions. This treatment dissolves away regions of low lateral order so that the water-insoluble, highly crystalline residue may be converted into a stable suspensoid by subsequent vigorous mechanical shearing action. The resulting nanocrystals occur as rod-like particles, whose dimensions depend on the nature of the substrate and hydrolysis conditions, but range in the nanometer scale [4].

However, the highly polar and hydrophilic character of polysaccharides and hydrophobic character of most of the polymeric matrices result in low interfacial

compatibility and performance of the final material. Some strategies have been suggested in the literature to improve the compatibility of polysaccharide nanocrystals with polymers [4–19].

In the present work, surface chemical modification involving grafting with organic acid chlorides presenting different lengths of the aliphatic chain was applied to ramie cellulose nanocrystals. The objective of this surface chemical treatment was to enhance the nonpolar nature of the grafted nanocrystals and improve their dispersibility in a nonpolar polymeric matrix. The morphology of the ensuing nanoparticles was characterized by microscopic observations and the crystallinity index was determined by X-ray diffraction.

2 MATERIALS AND METHODS

2.1 Materials

Ramie fibers were obtained from Stucken Melchers GmbH & Co. (Germany). Sulfuric acid (95%), triethylamine (TEA, 99.5%), toluene (anhydrous, 99.8%), acetone (99%), hexanoyl chloride, lauroyl chloride and stearoyl chloride (99%) were all obtained from Sigma-Aldrich.

*Corresponding author: jrmenezes@ufscar.br

DOI: 10.7569/JRM.2014.634121

2.2 Preparation of Cellulose Nanocrystals

Ramie fibers were first cut into small pieces and treated with a 2% NaOH solution at 80°C for 2 hours to remove residual additives. Then, the ramie fibers were submitted to an acid hydrolysis treatment with a 65 wt% H₂SO₄ solution at 55°C for 30 min under continuous stirring. The suspension was washed with water until neutral and dialyzed with deionized water. The obtained suspension was homogenized with an Ultra Turrax T25 homogenizer at 13,500 rpm (2–5 min) and then filtered in sintered glass N° 1.

2.3 Surface Chemical Modification of Cellulose Nanocrystals

The surface chemical modification of the cellulose nanocrystals was performed in a round-bottomed reaction flask under reflux (4 hours) and constant mechanical stirring in toluene medium. The toluene suspension was obtained using solvent exchange and centrifugation procedure (water to acetone, and then acetone to toluene, both four times). Ramie nanocrystals (2 g) were mixed with triethylamine (5 mL) and organic acid chloride (8 mL for hexanoyl, 10 ml for lauroyl or 13 mL for stearoyl chloride). Triethylamine was utilized to catalyze the reaction and as a complexing agent for HCl formed during the reaction [4]. The modified nanocrystals were submitted to a soxhlet extraction with acetone for 24 hours. The ramie cellulose nanocrystals modified with hexanoyl chloride, lauroyl chloride and stearoyl chloride will be denoted as WRC6, WRC12 and WRC18, respectively, whereas unmodified nanocrystals will be later on denoted as WRU.

2.4 Characterization

Fourier transform infrared spectroscopy: FTIR spectra were obtained on a Perkin-Elmer Paragon 1000 FTIR spectrometer. Both unmodified and chemically modified ramie cellulose nanocrystals were analyzed as KBr pellets (1:100).

X-ray diffraction: X-ray diffraction data were recorded for dry nanocrystals powders and LDPE-based nanocomposite films at room temperature with a Siemens D500 diffractometer equipped with a CuK α anode ($\lambda = 0.15406$ nm).

The crystallinity index, CI (%), was calculated by two different methods. First, from height ratio between the intensity of some specific peaks, following Equation 1 [20]:

$$CI (\%) = [(I_{002} - I_{am}) / I_{002}] \times 100 \quad (1)$$

where CrI expresses the relative degree of crystallinity, I_{002} is the intensity of the 002 lattice diffraction at $2\theta = 22.8^\circ$, and I_{am} is the intensity of diffraction at $2\theta = 18^\circ$. I_{002} represents both crystalline and amorphous regions, while I_{am} represents only the amorphous part.

In the second method, the individual peaks were extracted from X-ray diffraction patterns by peak fitting treatment from OriginPro7 program (OriginLab), considering Lorentz function for each peak, and CrI was calculated from the ratio of the area of all crystalline peaks to the total area [21]

The average thickness of cellulose crystallites was estimated from the X-ray diffraction patterns by Scherrer's Equation 2 [22,23]:

$$D_{hkl} = Kl / \beta_{1/2} \cos \theta \quad (2)$$

where D_{hkl} is the crystallite dimension in the direction normal to the hkl lattice planes family, K is the correction factor and usually taken as 0.9, λ is the radiation wavelength, θ is the diffraction angle and $\beta_{1/2}$ is the peak width at half maximum intensity.

Atomic force microscopy (AFM): AFM measurements were performed with an AFM Multimode-VS System, with Nanoscope V controller. All images were obtained in tapping mode, using Bruker's oxide-hardened Si tapping mode tips (TESPD). Typical spring constant for these tips is 20–80 N/m, with a nominal radius of curvature of 15 nm. The tapping amplitude was less than 4 nm and tip-sample contact time was minimal, so as to minimize the force exerted on the sample and therefore the influence of the scan on the aggregate morphology. A drop of diluted nanocrystal aqueous suspension, concentration of 0.5 mg/mL, was placed on an optical glass substrate, allowed to dry at room temperature and then analyzed by AFM.

Transmission electron microscopy (TEM): Drops of cellulose nanocrystal suspension were deposited on carbon-coated electron microscope grids and negatively stained with uranyl acetate solution. A Philips transmission electron microscope at an acceleration voltage of 80 kV was used.

Scanning electron microscopy with field emission gun (FEG-SEM): Drops of unmodified and modified cellulose nanocrystals suspensions, concentration of 0.5 mg/mL, in water and acetone, respectively, were deposited on carbon-coated electron microscope grids. The morphological characterization of the cellulose nanocrystals was performed with a SEM Zeiss Supra 35VP using ImageJ software to extract the pore counting and their radius.

3 RESULTS AND DISCUSSION

3.1 Characterization of Ramie Cellulose Nanocrystals

The rod-like nanocrystals resulting from acid hydrolysis of native ramie cellulose fibers exhibit an average diameter of 6–8 nm and a length of about 150–250 nm as estimated from atomic force micrographs.

In most cases, where both the very end and the wall of the tip contact circular samples, the Garcia model [24] should be applied. The Garcia model takes into account the asymmetry of the tip geometry and models the tip apex as two sloping walls with a sphere at their ends. In this case, the tip radius (R_T) is much less than the feature curvature radius (R_S) ($R_T \ll R_S$). In the case where only the very end of the tip contacts with the circular sample and tip apex are assumed to be a sphere, the Zenhausern model [25] can be applied to simplify the computation process; in this case, the tip radius is greater or approximately equal to the feature curvature radius ($R_T \geq R_S$). The model can be expressed as [26]:

$$W^2 = 16R_T R_S = 8R_T h \quad (3)$$

where W is the image width, R_T the radius of the tip apex, R_S the radius of the sample and h the sample (and also, the image) height (see Figure 2).

In order to be able to judge which of the models mentioned above should be used for a particular case, a critical value R_C is given by Equation 4:

$$R_C = R_T \frac{\sqrt{1 + (\tan(90^\circ - \theta))^2} - 1}{\sqrt{1 + (\tan(90^\circ - \theta))^2} + 1} \quad (4)$$

The Garcia model should be used when $R_S > R_C$, whilst the Zenhausern model should be used when $R_S \leq R_C$. For an ordinary AFM tip with tip radius of 15 nm (nominal value) and angle of sloping tip wall, the critical value R_C is calculated to be about 9 nm, and thus meets the condition for using the Zenhausern model instead of the Garcia model. Equation 3 can be used to predict the width of a molecule for a given radius of curvature of the tip. The corrected results for diameter of nanowhiskers were $R_S = 6.2 \pm 2.8$ nm. Bendahou *et al.* observed similar results, but with nanocrystals from the rachis of the date palm tree [27]. Similar results were obtained in the analysis of transmission electron microscopy (TEM) micrographs.

Figure 3A shows TEM micrographs of ramie cellulose nanocrystals. The length and diameter of

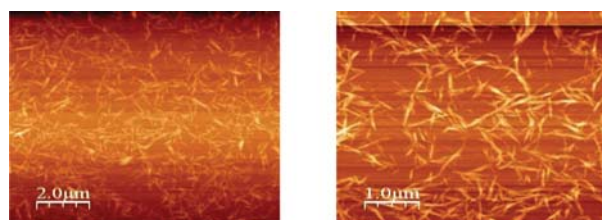


Figure 1 Atomic force micrograph of ramie cellulose nanocrystals.

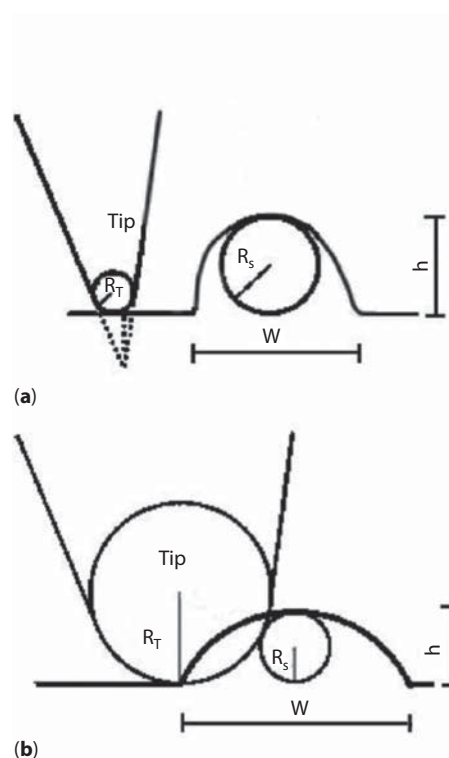


Figure 2 Illustration of lateral enlargement of AFM imaging in the case where only the tip radius curvature interacts with the sample (a) and for the case where both the tip apex and walls interact with the sample (b) [24].

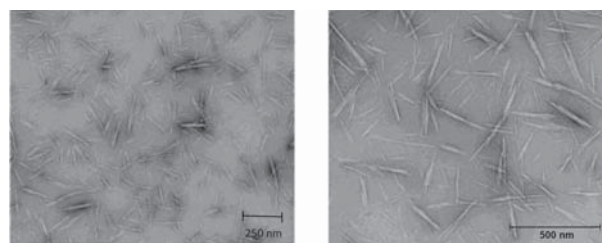


Figure 3 Transmission electron micrographs of ramie cellulose nanocrystals.

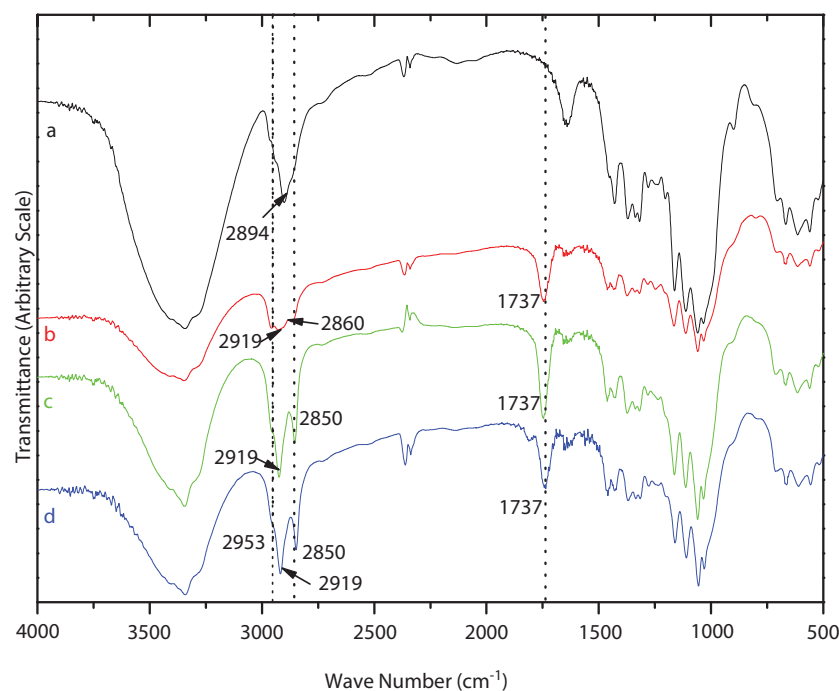


Figure 4 FTIR spectra (KBr pellets) of unmodified ramie cellulose nanocrystals (a) and modified with hexanoyl chloride (b), lauroyl chloride (c) and stearoyl chloride (d).

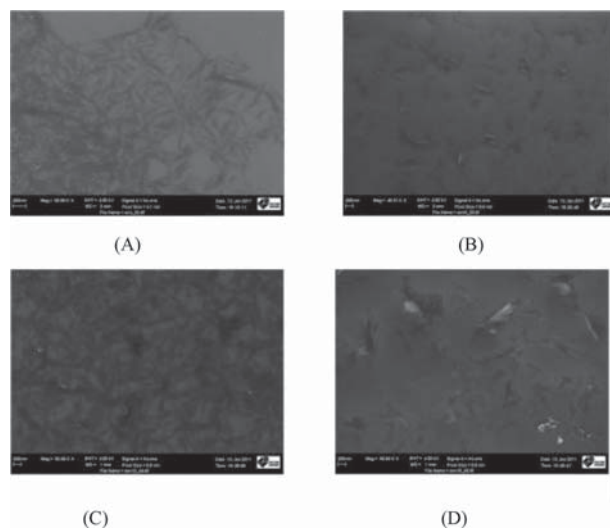


Figure 5 FEG-SEM of unmodified ramie cellulose nanocrystals (a) and modified with hexanoyl chloride (b), lauroyl chloride (c) and stearoyl chloride (d).

these nanocrystals were determined by using digital image analysis (ImageJ) [28]. The geometric average length and diameter were around $134 \text{ nm} \pm 59 \text{ nm}$ and $10.8 \text{ nm} \pm 4.5 \text{ nm}$, respectively, giving rise to an aspect ratio of around 12. A minimum of 228 and 70 measurements were used to determine the length and the diameter, respectively, of ramie whiskers. It is worth

noting that more than 50% of the nanoparticles have a length lower than 100 nm. Regarding their arrangement in solution, it is noteworthy that because of electrostatic repulsions between surface-grafted sulfate ester groups resulting from the sulfuric acid hydrolysis, the cellulose whiskers repel each other and then do not flocculate in water [28].

The FTIR spectra recorded for both unmodified and chemically modified ramie whiskers are shown in Figure 4. Compared to unmodified whiskers, the spectra corresponding to modified cellulose nanoparticles display a new peak at 1737 cm^{-1} , attributed to carbonyl groups. The signals at 2953 , 2919 and 2850 cm^{-1} are ascribed to the presence of grafted alkane chain. The concomitant decrease of the magnitude of the broad band around 3300 cm^{-1} for modified nanocrystals compared to unmodified nanocrystals is attributed to the partial disappearance of OH groups, confirming the success of the grafting reaction with organic acid chlorides.

Figure 5 shows FEG-SEM micrographs of cellulose nanocrystals. A similar morphology is observed for unmodified and modified nanocrystals with lauryl chloride in Figures 5a and 5c. Regarding their arrangement in suspension, it is noteworthy that because of electrostatic repulsions between surface-grafted sulfate ester groups resulting from the sulfuric acid hydrolysis, the cellulose nanocrystals repel each other and then do not flocculate in water. However,

the samples shown in Figures 5b and 5d, modified with hexanoyl chloride and stearoyl chloride, respectively, show significant changes in the morphology of the nanocrystals. A progressive build-up of a thermoplastic sleeve on the nanocrystal surface is expected. It is attributed to a higher degree of substitution (DS) for hexanoyl chloride (0.68) than for lauroyl and stearoyl chloride, that presented values of 0.32 and 0.31, respectively [28]. The DS values were obtained from elemental analysis results. Finally, the higher length for stearoyl chloride, sixteen carbon atoms, in relation to lauroyl chloride, twelve carbon atoms, probably makes the difference. In Figure 5B–D, cellulose nanocrystals seem to be linked in larger aggregates. Threads linking cellulose nanoparticles are supposed to be composed of grafted chains.

Natural lignocellulosic fibers are known to display X-ray diffraction (XRD) patterns typical of type I cellulose, with the main diffraction signals at 2θ values of 15° , 16° , 22.5° and 34° , attributed to the diffraction planes 101, $10\bar{1}$, 002 and 040, respectively. Figure 6 shows the XRD patterns obtained for the modified ramie cellulose nanocrystals samples as well as the

one corresponding to the pristine sample. Even after chemical modification, the cellulosic nanoparticles remain semicrystalline and display the same XRD patterns leading to the conclusion that the initial crystallinity was retained. Then, the surface chemical modification did not alter the crystallinity of cellulose nanocrystals. After chemical modification, a new peak that appears around 21° that is attributed to the crystallization of grafted aliphatic chains. The crystalline index calculated from the Segal method gives values of 88.3, 85.7, 82.6 and 85.0 for unmodified nanocrystals, and modified with C6, C12 and C18, respectively.

By using Scherrer's equation (Equation 2) the crystal size perpendicular to the 002 planes was determined. For this, X-ray data were normalized and then the main peaks with the same y-axis values could be compared directly. Figure 7 shows the deconvoluted XRD data and from this the peak width at half maximum intensity ($\beta_{1/2}$) was obtained and the crystallite dimension was calculated. The obtained results are 6.2 nm, 6.3 nm, 6.1 nm and 6.3 nm for unmodified cellulose nanocrystals, and modified with C6, C12 and C18, respectively. These values are very close to those

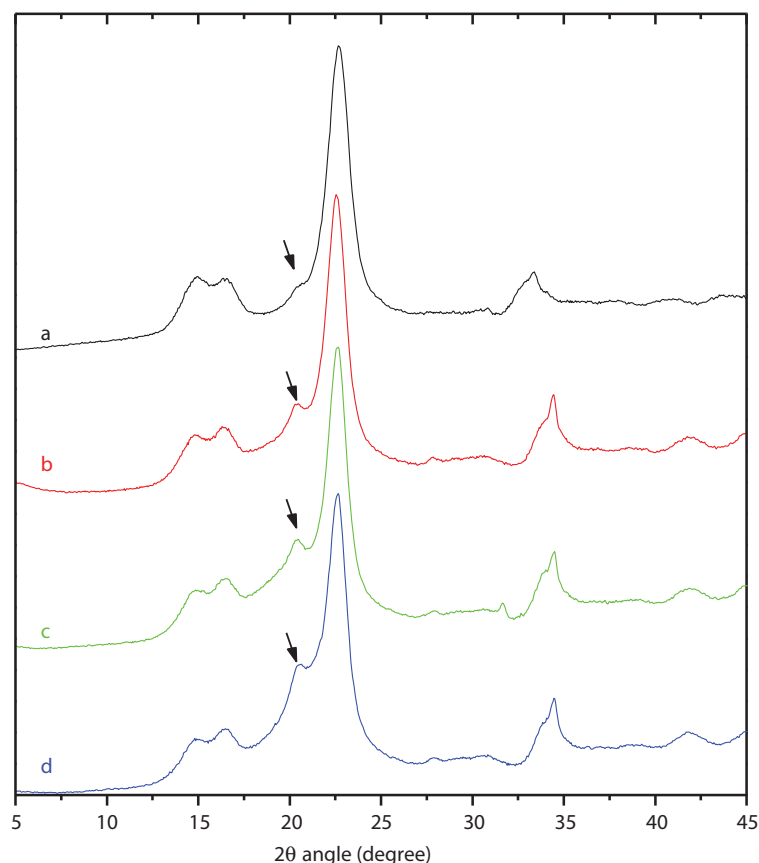


Figure 6 X-ray diffraction patterns for unmodified ramie cellulose nanocrystals (a) and modified with hexanoyl chloride (b), lauroyl chloride (c) and stearoyl chloride (d).

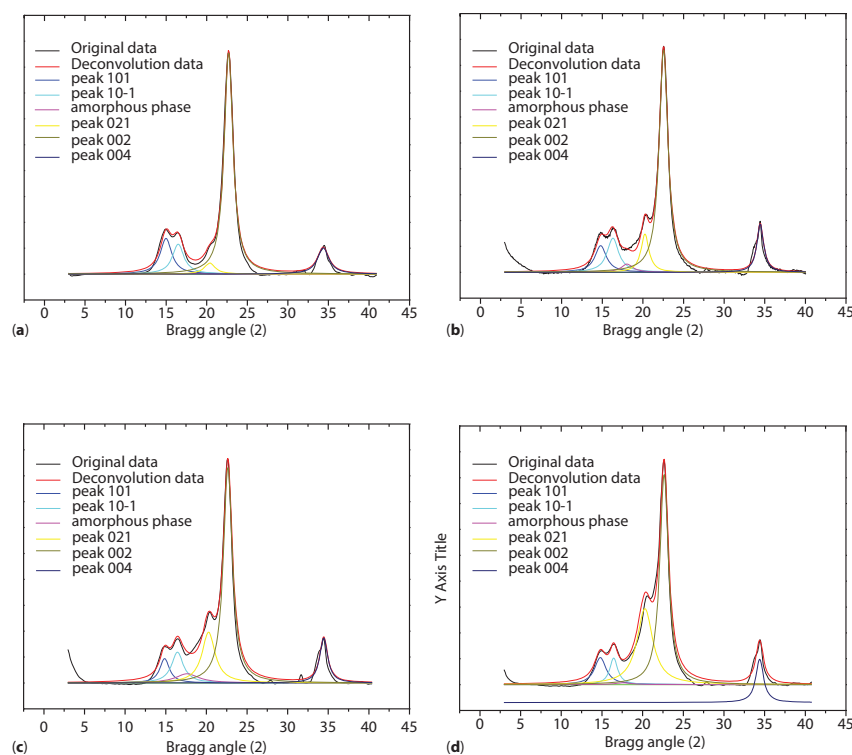


Figure 7 X-ray diffraction patterns and peak deconvolution for unmodified ramie cellulose nanocrystals (a) and modified with hexanoyl chloride (b), lauroyl chloride (c) and stearoyl chloride (d).

determined from AFM observations indicating, in this case, that AFM measurement is more accurate than TEM.

From Figure 7 and using five Lorentz crystalline peaks (101, 10-1, 021, 002 and 040) CI was calculated from the ratio of the area of all crystalline peaks to the total area. Values of 99.78, 97.27, 94.83 and 99.29% were obtained for unmodified cellulose nanocrystals and modified with C6, C12 and C18, respectively. The higher values obtained compared to those obtained from the Segal method can be attributed to the contribution of the several peaks, because in the Segal method only the highest peak (002) is used in the calculation. This excludes contributions from the other crystalline peaks. The increase of the 021 peak, attributed to aliphatic chain contribution, can also be observed in Figure 7. The results were found to be 9.16, 17.21 and 29.40% for cellulose nanocrystals modified with C6, C12 and C18, respectively.

4 CONCLUSIONS

The surface of cellulose nanocrystals prepared by acid hydrolysis of ramie fibers was chemically modified using organic acid chloride aliphatic chains of different sizes, namely hexanoyl chloride, lauroyl chloride

and stearoyl chloride. The evidence of occurrence of chemical modification was checked by FTIR. X-ray diffraction analysis was used to check that the initial crystalline structure was preserved. The morphological characteristics of ramie nanocrystals were successfully characterized by FEG-SEM, AFM and TEM. The different microscopy techniques provide similar results regarding the morphology and geometrical dimensions of the nanocrystals. However, significant differences were reported for the determination of their crystallinity index from X-ray diffraction patterns. The deconvolution method leads to much higher values than the Segal method.

ACKNOWLEDGEMENTS

A. J. de Menezes thanks the CAPES (Brazil) for post-doctoral scholarship and FAPESP for financial support 2014/02416-2 and F. L. Leite thanks FAPESP for financial support 07/05089-9.

REFERENCES

1. B. Wang, M. Sain, and K. Oksman, Study of structural morphology of hemp fiber from the micro to the nanoscale. *Appl. Compos. Mater.* **14**, 89–103 (2007).

2. M.A.S. Azizi Samir, F. Alloin, and A. Dufresne, Review of recent research into cellulosic whiskers, their properties and their application in nanocomposite field. *Biomacromolecules* **6**(2), 612–626 (2005).
3. A. Dufresne, Comparing the mechanical properties of high performances polymer nanocomposites from biological sources. *J. Nanosci. Nanotechnol.* **6**(2), 322–330 (2006).
4. A. Dufresne, *Nanocellulose: From Nature to Higherperformance Tailored Materials*, p. 147, De Gruyter, Berlin-Germany (2012).
5. Y. Habibi, L.A. Lucia, and O.J. Rojas, Cellulose nanocrystals: Chemistry, self-assembly, and applications. *Chem. Rev.* **110**, 3479–3500 (2010).
6. W. Thielemans, M.N. Belgacem, and A. Dufresne, Starch nanocrystals with large chain surface modifications. *Langmuir* **22**(10), 4804–4910 (2006).
7. M. Labet, W. Thielemans, and A. Dufresne, Polymer grafting onto starch nanocrystals. *Biomacromolecules* **8**(9), 2916–2927 (2007).
8. I. Sakurada, Y. Nukushina, and T. Ito, Experimental determination of the elastic modulus of crystalline regions in oriented polymers. *J. Polym. Sci.* **57**, 651–660 (1962).
9. K. Tashiro and M. Kobayashi, Theoretical evaluation of three-dimensional elastic constants of native and regenerated celluloses: Role of hydrogen bonds. *Polymer* **32**, 1516–1526 (1991).
10. A. Šturcová, G.R. Davies, and S.J. Eichhorn, Elastic modulus and stress-transfer properties of tunicate cellulose whiskers. *Biomacromolecules* **6**, 1055–1061 (2005).
11. M.N. Anglès and A. Dufresne, Plasticized starch/tunicin whiskers nanocomposites. 1. Structural analysis. *Macromolecules* **33**, 8344–8353 (2000); A.P. Mathew and A. Dufresne, Morphological investigation of nanocomposites from sorbitol plasticized starch and tunicin whiskers. *Biomacromolecules* **3**, 609–617 (2002); W.J. Orts, J. Shey, S.H. Imam, G.M. Glenn, M.E. Guttman, and J.F. Revol, Application of cellulose microfibrils in polymer nanocomposites. *J. Polym. Env.* **13**, 301–306 (2005); I. Kvien, J. Sugiyama, M. Votrubeč, and K. Oksman, Characterization of starch based nanocomposites. *J. Mater. Sci.* **42**, 8163–8171 (2007); M.A.S. Azizi Samir, F. Alloin, J.Y. Sanchez, and A. Dufresne, Cellulose nanocrystals reinforced poly (oxyethylene). *Polymer* **45**, 4033–4041 (2004); M.A.S. Azizi Samir, F. Alloin, W. Gorecki, J.Y. Sanchez, and A. Dufresne, Nanocomposite polymer electrolytes based on poly (oxyethylene) and cellulose nanocrystals. *J. Phys. Chem. B* **108**, 10845–10852 (2004); M.A.S. Azizi Samir, A. Montero Mateos, F. Alloin, J.Y. Sanchez, and A. Dufresne, Plasticized nanocomposite polymer electrolytes based on poly (oxyethylene) and cellulose whiskers. *Electrochim. Acta* **49**, 4667–4677 (2004); M.A.S. Azizi Samir, L. Chazeau, F. Alloin, J.Y. Cavaille, A. Dufresne, and J.Y. Sanchez, POE-based nanocomposite polymer electrolytes reinforced with cellulose whiskers. *Electrochim. Acta* **50**, 3897–3903 (2005); M.A.S. Azizi Samir, F. Alloin, and A. Dufresne, High performance nanocomposite polymer electrolytes. *Compos. Interfaces* **13**, 545–559 (2006), T. Zimmermann, E. Pöhler, and T. Geiger, Cellulose fibrils for polymer reinforcement. *Adv. Eng. Mat.* **6**, 754–761 (2004); T. Zimmermann, E. Pöhler, and P. Schwaller, Mechanical and morphological properties of cellulose fibril reinforced nanocomposites. *Adv. Eng. Mat.* **7**, 1156–1161 (2005); Y.J. Choi and J. Simonsen, Cellulose nanocrystal-filled carboxymethyl cellulose nanocomposites. *J. Nanosci. Nanotechnol.* **6**, 633–639 (2006).
12. V. Favier, G.R. Canova, J.Y. Cavaille, H. Chanzy, A. Dufresne, and C. Gauthier, Nanocomposite materials from latex and cellulose whiskers. *Polym. Adv. Technol.* **6**, 351–355 (1995); W. Helbert, J.Y. Cavaille, and A. Dufresne, Thermoplastic nanocomposites filled with wheat straw cellulose whiskers. Part I: processing and mechanical behavior. *Polym. Compos.* **17**, 604–611 (1996); A. Dufresne, J.Y. Cavaille, and W. Helbert, Thermoplastic nanocomposites filled with wheat straw cellulose whiskers. Part II: effect of processing and modeling. *Polym. Compos.* **18**, 198–210 (1997); D. Dubief, E. Samain, and A. Dufresne, Polysaccharide microcrystals reinforced amorphous poly (β -hydroxyoctanoate) nanocomposite materials. *Macromolecules* **32**, 5765–5771 (1999); A. Dufresne, M.B. Kellerhals, and B. Witholt, Transcrystallization in Mcl-PHAs/cellulose whiskers composites. *Macromolecules* **32**, 7396–7401 (1999); A. Dufresne, Dynamic mechanical analysis of the interphase in bacterial polyester/cellulose whiskers natural composites. *Compos. Interfaces* **7**, 53–67 (2000); L. Chazeau, J.Y. Cavaille, G.R. Canova, R. Dendievel, and B. Boutherein, *J. Appl. Polym. Sci.* **71**, 1797–1808 (1999); L. Chazeau, J.Y. Cavaille, and P. Terech, Mechanical behaviour above T_g of a plasticized PVC reinforced with cellulose whiskers; a SANS structural study. *Polymer* **40**, 5333–5344 (1999); L. Chazeau, M. Paillet, and J.Y. Cavaille, Plasticized PVC reinforced with cellulose whiskers. I. Linear viscoelastic behavior analyzed through the quasi-point defect theory. *J. Polym. Sci. B: Polym. Phys.* **37**, 2151–2164 (1999); L. Chazeau, J.Y. Cavaille, and J. Perez, Plasticized PVC reinforced with cellulose whiskers. II. Plastic behavior. *J. Polym. Sci. B: Polym. Phys.* **38**, 383–392 (2000); M. Matos Ruiz, J.Y. Cavaille, A. Dufresne, C. Graillat, and J.F. Gerard, New waterborne epoxy coatings based on cellulose nanofillers. *Macromol. Symp.* **169**, 211–222 (2001); N.L. Garcia de Rodriguez, W. Thielemans, and A. Dufresne, Sisal cellulose whiskers reinforced polyvinyl acetate nanocomposites. *Cellulose* **13**, 261–270 (2006).
13. L. Heux, G. Chauve, and C. Bonini, Nonflocculating and chiral-nematic self-ordering of cellulose microcrystals suspensions in nonpolar solvents. *Langmuir* **16**, 8210–8212 (2000); I. Kvien, S.T. Bjom, and K. Oksman, Characterization of cellulose whiskers and their nanocomposites by atomic force and electron microscopy. *Biomacromolecules* **6**, 3160–3165 (2005).
14. C. Goussé, H. Chanzy, G. Exoffier, L. Soubeyrand, and E. Fleury, Stable suspensions of partially silylated cellulose whiskers dispersed in organic solvents. *Polymer* **43**, 2645–2651 (2002); K. Gopalan Nair, A. Dufresne, A. Gandini, and M.N. Belgacem, Crab shell chitin

- whiskers reinforced natural rubber nanocomposites. 3. Effect of chemical modification of chitin whiskers. *Biomacromolecules* **4**, 1835–1842 (2003); H. Angellier, S. Molina-Boisseau, M.N. Belgacem, and A. Dufresne, Surface chemical modification of waxy maize starch nanocrystals. *Langmuir* **21**, 2425–2433 (2005).
15. M.A.S. Azizi Samir, F. Alloin, J.Y. Sanchez, N. El Kissi, and A. Dufresne, Preparation of cellulose whiskers reinforced nanocomposites from an organic medium suspension. *Macromolecules* **37**, 1386–1393 (2004); N.E. Marcovich, M.L. Auad, N.E. Belessi, S.R. Nutt, and M.I. Aranguren, Cellulose micro/nanocrystals reinforced polyurethane. *J. Mater. Res.* **21**, 870–881 (2006); O. van den Berg, J.R. Capadona, and C. Weder, A versatile approach for the processing of polymer nanocomposites with self-assembled nanofibre templates. *Biomacromolecules* **18**, 1353–1357 (2007).
 16. A.N. Nakagaito and H. Yano, The effect of morphological changes from pulp fiber towards nano-scale fibrillated cellulose on the mechanical properties of high-strength plant fiber based composites. *Appl. Phys. A* **78**, 547–552 (2004); A.N. Nakagaito, S. Iwamoto, and H. Yano, Bacterial cellulose: The ultimate nano-scalar cellulose morphology for the production of high-strength composites. *Appl. Phys. A* **80**, 155–159 (2005); A.N. Nakagaito and H. Yano, The effect of fiber content on the mechanical and thermal expansion properties of biocomposites based on microfibrillated cellulose. *Cellulose* **15**, 323–331 (2008); Y. Shimazaki, Y. Miyazaki, Y. Takezawa, M. Nogi, K. Abe, S. Ifuku, and H. Yano, Excellent thermal conductivity of transparent cellulose nanofiber/epoxy resin nanocomposites. *Biomacromolecules* **8**, 2976–2978 (2007); H. Yano, J. Sugiyama, A.N. Nakagaito, M. Nogi, T. Matsuura, M. Hikita, and K. Handa, Optically transparent composites reinforced with networks of bacterial nanofibers. *Adv. Mat.* **17**, 153–155 (2005); M. Nogi, K. Handa, A.N. Nakagaito, and H. Yano, Optically transparent bionanofiber composites with low sensitivity to refractive index of the polymer matrix. *Appl. Phys. Lett.* **87**, 243110 (2005); S. Iwamoto, K. Abe, and H. Yano, The effect of hemicelluloses on wood pulp nanofibrillation and nanofiber network characteristics. *Biomacromolecules* **9**, 1022–1026 (2008); M. Henriksson and L.A. Berglund, Structure and properties of cellulose nanocomposite films containing melamine formaldehyde. *J. Appl. Polym. Sci.* **106**, 2817–2824 (2007).
 17. K. Oksman, A.P. Mathew, D. Bondeson, and I. Kvien, Manufacturing process of cellulose whiskers/poly(lactic acid) nanocomposites. *Compos. Sci. Technol.* **66**, 2776–2784 (2006).
 18. D. Bondeson and K. Oksman, Poly(lactic acid)/cellulose whisker nanocomposites modified by poly(vinyl alcohol). *Compos. Part A* **38**, 2486–2492 (2007).
 19. Y. Habibi, A.L. Goffin, N. Schiltz, E. Duquesne, P. Dubois, and A. Dufresne, Bionanocomposites based on poly(ϵ -caprolactone)-grafted cellulose nanocrystals by ring-opening polymerization. *J. Mater. Chem.* **18**, 5002–5010 (2008).
 20. L. Segal, J.J. Creely, A.E. Martin, and C.M. Conrad, An empirical method for estimating the degree of crystallinity of native cellulose using the X-ray diffractometer. *Textile Res. J.* **29**, 786–793 (1959).
 21. S. Park, J.O. Baker, M.E. Himmel, P.A. Parilla, and D.K. Johnson, Cellulose crystallinity index: Measurement techniques and their impact on interpreting cellulase performance. *Biotechnol. Biofuels* **3**(10), 1–10 (2010).
 22. H.P. Klug and L.E. Alexander, *X-ray Diffraction Procedures for Polycrystalline and Amorphous Materials*. John Wiley & Sons, NY. (1974).
 23. B.D. Cullity. *Elements of X-ray diffraction*. Addison-Wesley Publishing Company, Inc., Second edition, MA. (1978).
 24. V.J. Garcia, L. Martinez, J.M. Briceno-Valero, and C.H. Schilling, Dimensional metrology of nanometric spherical particles using AFM: I, model development. *Probe Microsc.* **1**, 107–116 (1997).
 25. F. Zenhausern, M. Adrian, B.T. Heggeler-Bordied, I.M. Eng, and P. Descouts, DNA and RNA polymerase/DNA complex imaged by scanning force microscopy. *Scanning.* **14**, 212 (1992).
 26. Y. Wang and X. Chen, *Ultramicroscopy* **107**, 293–298 (2007).
 27. A. Bendahou, A. Hajlane, A. Dufresne, and A. Kaddami, Esterification and amidation for grafting long aliphatic chains on to cellulose nanocrystals: A comparative study. *Res. Chem. Intermed* (2014) DOI 10.1007/s11164-014-1530-z.
 28. A.J. De Menezes, G. Siqueira, A.A.S. Curvelo, and A. Dufresne, Extrusion and characterization of functionalized cellulose whiskers reinforced polyethylene nanocomposites. *Polymer* **50**, 4552–4563 (2009).